Numerical Simulation of Damage Behaviour of Textile Reinforced Composites in Aircraft Structures

Peter Linde[*], Peter Middendorf[**], Björn Van Den Broucke[**], Henk de Boer[***]
[*]Airbus Operations GmbH, [**]EADS IW-G, [***]Advanced Lightweight Engineering
Keywords: textile reinforcement, computer tomography, representative volume element, multi scale model, user subroutine

Abstract

In the design of civil aircraft an increase in use of carbon fibre composites as a structural material of the airframe has taken place during the last decades.

To obtain a more complete carbon composites airframe, it will necessary to manufacture and use more versatile stiffening elements of this material.

Composites parts with three dimensional fibre reinforcement are becoming increasingly interesting as an alternative to joining several skin layers, or joining separate stiffeners onto skin. The 3D fibre reinforcement improves the ability to take up loads acting on the part in out-of-plane directions. At the same time a certain reduction in longitudinal performance is observed, in particular in compression. Although the most recent 3D composites have improved in this respect, it is nevertheless of high importance to understand the structural behavior of these parts and to be able to predict the behavior und mechanical loading up to failure.

This paper deals with a numerical model for the simulation of the damage behaviour of textile reinforced carbon composites under static loading. The developments described here form a first part in a program intended to deal with several fibre architectures. Here focus is placed on braided architecture with a newly developed model. The model employs a multi-scale approach, and characterizes the fibre architecture by a "Representative Volume Element" (RVE), in this study aided by micro computer tomography. Constitutive model, failure criteria and damage behaviour are formulated on the meso-scale level. To enable practical engineering use the behavior of the RVE is scaled up to macro level by homogenization. The formulation is implemented in a user subroutine in the nonlinear finite element program ABAQUS and is developed for industrial use. Validation is performed versus basic test results. Finally a summary, conclusions and recommendations for future research are presented.

1 Introduction

Integrated 3D composite parts are on their way of becoming the solution of choice at locations where hitherto several parts were joined to each other. The joining often occurs with fasteners, that are not only heavy; when their large numbers are taken into account; the fastening is furthermore not advantageous out of fatigue point of view.

Advances made recently in infusion techniques and in the fibre architecture make the use of 3D textile reinforced parts increasingly attractive. The advantages of these, versus repeated use of doublers, and riveting stiffening parts together, lies in the fact that the 3D textile reinforced parts may replace many parts with one and in addition fasteners may be omitted. Aircraft architects correspondingly favour increased used of these parts in aircraft in planning.

a) 2D Braided fibre architecture

b) 3D woven fibre architectire

c) Non crimp fabric (NCF)
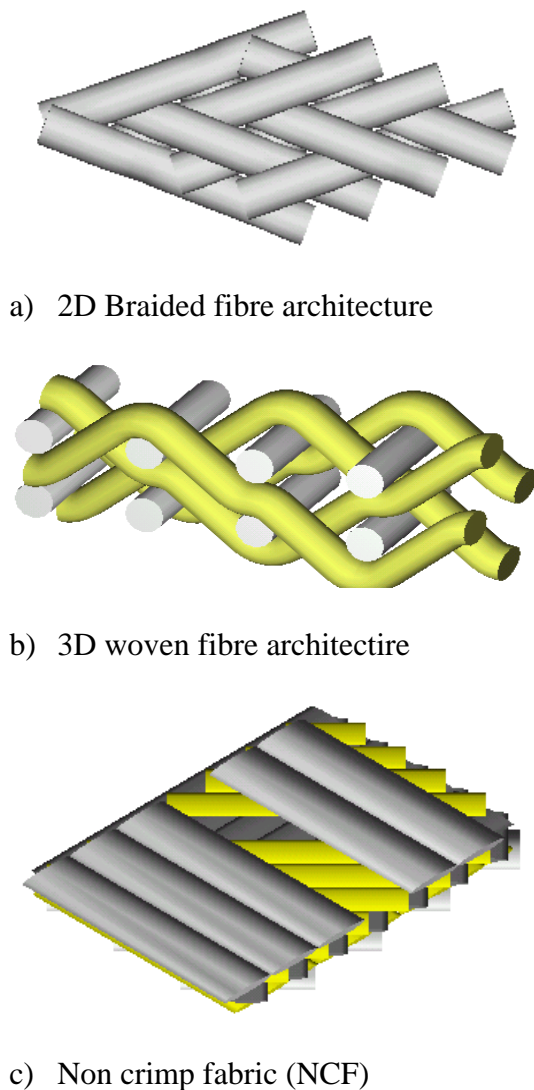
Fig. 1. Examples of 3D fibre architectures

The 3D textile reinforcement may contribute significantly to the strength of the part in out-of-plane directions, depending on the used fiber architecture. It is of high importance to understand this strength and to be able to predict it in a reliable manner. Furthermore, 3D textile reinforced parts will usually be subjected to a certain reduction in the in-plane strength and stiffness, which is equally important to assess and predict, in particular under compression, not at least since this may affect the stability behavior.

More advanced fibre architectures are developed. In general 3D "textile reinforced" composites, depending on definition, may include fiber architectures, such as; braided, woven, NCF, tufted, and to some degree stitched and pinned.

In this paper the sequence of work will be treated of industrial research aiming at a practical industrially useable numerical model for the simulation of the nonlinear structural behavior of 3D composites subjected top mechanical loading, up through the damage region until structural failure.

The work described here builds on research carried out in a cooperation between the Katholieke Universiteit Leuven [1], and the EADS Innovation Works, dealing with the formulation of the fiber architecture and its implementation into a finite element based environment, named WiseTex. In a subsequent stage EADS IW with ALE undertook some steps towards industrialization for engineering simulation purposes in cooperation with Airbus [2].

The focus in this paper is on braided fiber architecture, evaluated to be of interest for aircraft applications not at least due to its improved behavior in connection with impact damages, compared to uni-directional layered composites. Due to its relative large ratio of in-plane fiber components, this is sometimes referred to as "2,5D" fiber reinforcement.

The scope of the paper is as follows: Upon the introduction a general strategy for the numerical model is presented. This is followed by treatment of the representative volume element (RVE), and the characterization of the fibre directions by computer tomography. The implementation of a damage model is then discussed, followed by the periodic boundary conditions. An example of simulation with the RVE for a selected braided composite is then shown. Thereupon next development steps are discussed. Finally; a summary, conclusions and recommendations are presented.
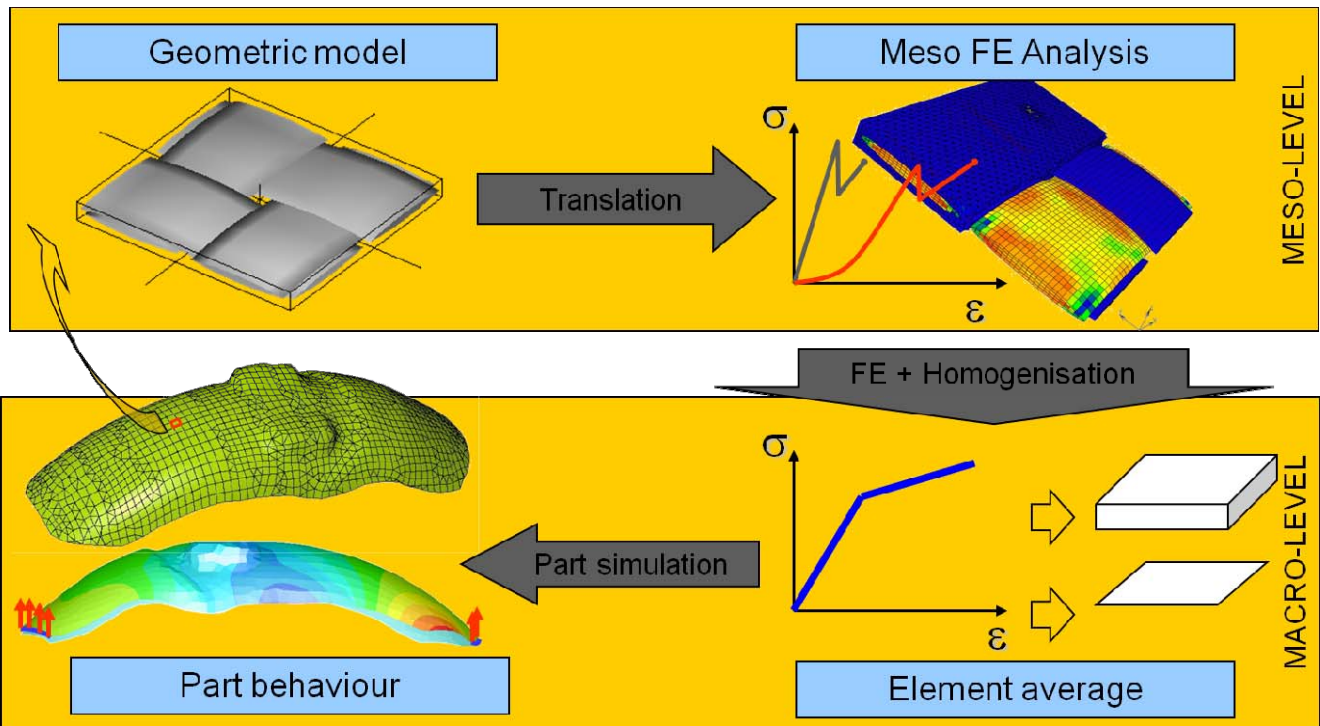
Figure 2.1 Strategy for multi-scale modeling

2 Numerical model

2.1 Modelling strategy

A multi-scale modeling approach is used, shown in Fig. 2.1. The smallest volume that contains the necessary part of recurring fibres in order to capture the 3D stiffness is determined, as the representative volume element, RVE. It is seen in the figure as a geometry model on top to the left, and on top to the right with the yarns and the matrix both meshed with solid elements.

Both constituents; fibres and matrix are supplied with a material model each. This should be a nonlinear model with damage behavior.

In order to utilize the model in realistic engineering simulations, it is necessary to be able to use it in typical finite elements, of the type being used for skins, stringers, etc. For this purpose a homogenization is carried out, so that the behavior of the RVE is transferred up to the macro level (see bottom right in Fig. 2. Typcial elements may be solids or continuum shells.

With these elements the part to be analysed (see Fig. 2.1, bottom, left) is now modeled and will be able to be analysed realistically, yet efficiently.

2.2 Computer tomography

In order to be able to readily capture the 3D fibre geometry of an arbitrary fibre architecture, the EADS-IW developed an approach based on micro computer tomography, CT, [3] in which the fibre geometry is measured in direct scanning.
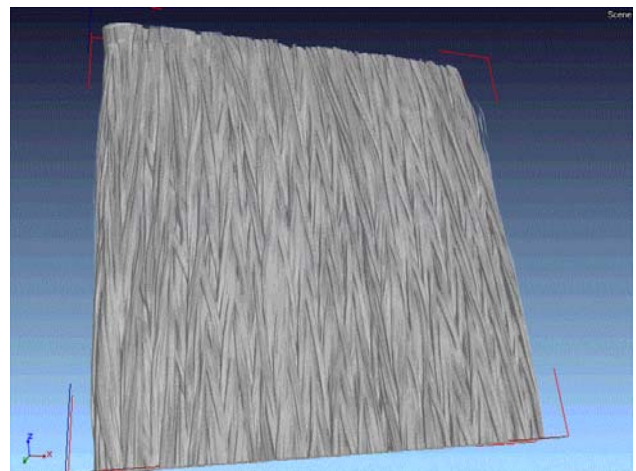
Fig. 2.2 Dry fiber braided reinforcement
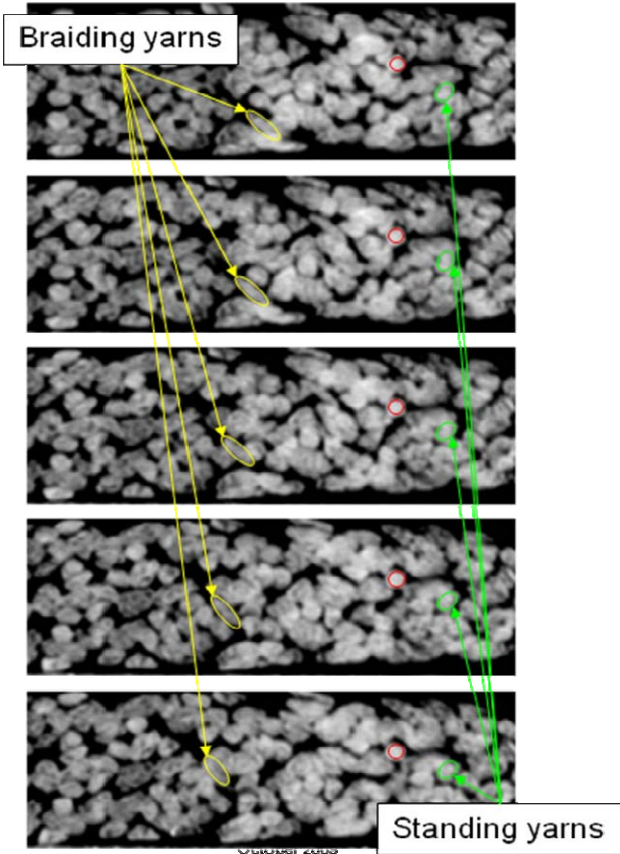
Fig. 2.3 Cross sectional micro CT scans

Directly upon that the captured fibre geometry is connected to Altair Hypermesh, in which a corresponding 3D geometry is generated. In Fig. 2.2 a dry fiber braided reinforcement for a square plate is seen, which was placed in the computer tomography. Fig. 2.3 shows CT images taken as cross-sectional images at consecutive locations. Two yarns are tracked through all the cross-sections, one "braiding yarn (marked in yellow), and one "standing year (marked in red). In Fig. 2.4 a 3D image is shown of the same specimen, in the form of a contour plot, with the fiber angles as variable.

Until micro CT was introduced the establishment of a realistic RVE was a very complex process, involving geometrical data from the manufacturer, discussed in [2] that now has become considerably simplified, and more reliable. The geometry and meshing into solid elements is established in Hypermesh for subsequent simulation in ABAQUS.
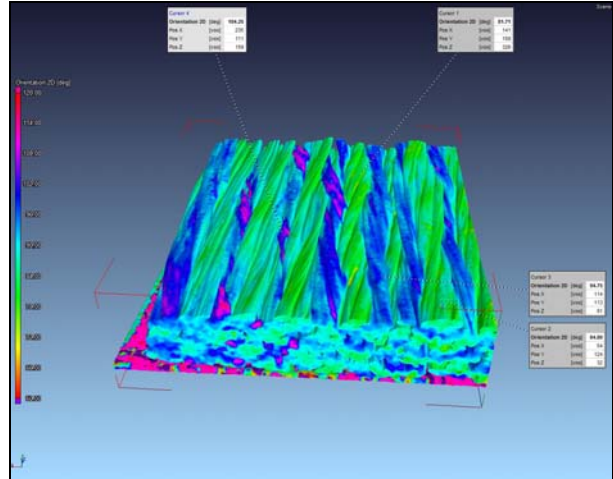
Fig. 2.4 3D micro CT scan of braided fiber reinforcement

2.3 Material models

The yarns (fibers bundles) obtain their fibre longitudinal (0 degree) orientation along the yarn center directions and a variable fibre volume fraction according to used yearn (typically appr 60 % in yarn center and decreasing outwards down to appr 50 % at yearn edge). The material model for the yarns is as follows

$$
\begin{bmatrix} \varepsilon_{11} \\ \varepsilon_{22} \\ \varepsilon_{33} \\ \varepsilon_{12} \\ \varepsilon_{13} \\ \varepsilon_{23} \end{bmatrix} = \begin{bmatrix} \dfrac{1}{E_l} & -\dfrac{v_{tl}}{E_t} & -\dfrac{v_{tl}}{E_t} & 0 & 0 & 0 \\ -\dfrac{v_{lt}}{E_l} & \dfrac{1}{E_t} & -\dfrac{v_t}{E_t} & 0 & 0 & 0 \\ -\dfrac{v_{lt}}{E_l} & -\dfrac{v_t}{E_t} & \dfrac{1}{E_t} & 0 & 0 & 0 \\ 0 & 0 & 0 & \dfrac{1}{G_l} & 0 & 0 \\ 0 & 0 & 0 & 0 & \dfrac{1}{G_l} & 0 \\ 0 & 0 & 0 & 0 & 0 & \dfrac{1}{G_t} \end{bmatrix} \begin{bmatrix} \sigma_{11} \\ \sigma_{22} \\ \sigma_{33} \\ \sigma_{12} \\ \sigma_{13} \\ \sigma_{23} \end{bmatrix} = C\sigma
\tag{1}
$$

Here subscript l indicates the longitudinal direction and subscript t denotes transverse direction. Fibre related damage is accounted for by a scalar damage parameter d_l. The Young's modulus is defined as a function of this damage parameter as follows:

$$
E_l = E_l^0 (1 - d_l)
\tag{2}
$$

where the initial stiffness E_l^0 is defined as the stiffness of the material when no damage is present. In addition, a distinction between tensile and compressive mode is made by defining a tensile E_l^{0t} and compressive E_l^{0c} modulus. The nonlinear behaviour in compression is defined as:

$$E_l^\gamma = \frac{E_l^{0c}}{1 + \gamma E_l^{0c}|\varepsilon_{11}|} \tag{3}$$

Matrix related damage is taken into account by two scalar parameters d_t and d_s. Parameter d_s is related to debonding of fibre and matrix

whereas d_t accounts for transverse micro-cracking. The engineering constants are

$$E_t = E_t^0(1 - d_t)$$
$$G_t = G_t^0(1 - d_t) = \frac{E_t^0}{2(1 + v_{lt})}(1 - d_t) \tag{4}$$
$$G_l = G_l^0(1 - d_s)$$

The strain energy density function of the material is given by:

$$W = \frac{1}{2(1 - d_l)}\left[\frac{\langle\sigma_{11}\rangle^2}{E_l^{0t}} + \frac{\Psi\langle-\sigma_{11}\rangle^2}{E_l^{0c}}\right] - $$
$$\frac{1}{2(1 - d_l)}\left(\frac{v_{lt}}{E_l^0} + \frac{v_{tl}}{E_t^0}\right)\sigma_{11}(\sigma_{22} + \sigma_{33})$$
$$+ \frac{\langle-\sigma_{22}\rangle^2 + \langle-\sigma_{33}\rangle^2}{E_t^0} + \frac{1}{2(1 - d_s)}\left[\frac{\sigma_{44}^2 + \sigma_{55}^2}{G_l^0}\right]$$
$$\frac{1}{2(1 - d_t)}\left[\frac{\langle-\sigma_{22}\rangle^2 + \langle-\sigma_{33}\rangle^2}{E_t^0} + \frac{2v_t}{E_t^0}\sigma_{22}\sigma_{33} + \frac{\sigma_{66}^2}{G_t^0}\right] \tag{5}$$

where $\langle\ \rangle$ denote Mc Auley brackets. The thermodynamic equivalent forces associated to the damage parameters are defined as:

$$Z_l = \frac{\partial W}{\partial d_l} = \frac{1}{2(1 - d_l)^2}\left[\frac{\langle\sigma_{11}\rangle^2}{E_l^{0t}} + \frac{\Psi\langle-\sigma_{11}\rangle^2}{E_l^{0c}}\right] - $$

$$\frac{1}{2(1 - d_l)^2}\left(\frac{v_{lt}}{E_l^0} + \frac{v_{tl}}{E_t^0}\right)\sigma_{11}(\sigma_{22} + \sigma_{33}) \tag{6a}$$

$$Z_t = \frac{\partial W}{\partial d_t} = \frac{1}{2(1 - d_t)^2}\frac{\langle-\sigma_{22}\rangle^2 + \langle-\sigma_{33}\rangle^2}{E_t^0} + $$

$$\frac{1}{2(1 - d_t)^2}\left[-\frac{2v_t}{E_t^0}\sigma_{22}\sigma_{33} + \frac{\sigma_{66}^2}{G_t^0}\right] \tag{6b}$$

$$Z_s = \frac{\partial W}{\partial d_s} = \frac{1}{2(1 - d_s)^2}\left[\frac{\sigma_{44}^2 + \sigma_{55}^2}{G_l^0}\right] \tag{6c}$$

Damage evolution is based on the following active damage forces:

$$Y_l = \max\sqrt{Z_l(\tau)} \tag{7a}$$

$$Y_t = \max\sqrt{Z_t(\tau)} \tag{7b}$$

$$Y_s = \max\sqrt{Z_s(\tau) + b\,Z_t(\tau)} \tag{7c}$$

Here b is a material parameter that provides a coupling between transverse and shear energies. The relation between damage parameters and active damage forces is given by:

$$d = \begin{cases} 0 & \text{if} & Y < Y^0 \\ \dfrac{Y - Y^0}{Y^C} & \text{if} & Y^0 \le Y \le Y^L \\ d_{max} - \left(\dfrac{Y^L}{Y}\right)^\alpha\left(d_{max} - \dfrac{Y^L - Y^0}{Y^C}\right) & \text{if} & Y^L < Y \end{cases} \tag{8}$$

The exponential form of d if $Y > Y^L$ is introduced to improve convergence.

The practical implementation of the procedure using the equations 1 to 8 can be summarized as follows:

1. Get current strain and get stress of previous increment (input values)
2. Get previous value of damage

parameters
3. Start iteration to compute damage parameters
   a. Calculate thermodynamic forces (Eq. 6 & 7)
   b. Calculate damage parameters (Eq. 8)
   c. Stop iteration when damage parameters have converged
4. Compute C and update stress (Eq. 1)
5. Use inverse of C as Jacobian

Within the third step the stress from the last converged increment is used.
In the third step of the procedure converged stresses from the previous increment are used. An improvement would be to use updates stresses, as functions of strains and damage parameters.
With such an improvement, the procedure would look as follows:

1. Get current strain (input value)
2. Get previous value of damage parameters
3. Compute current stress (Eq. 1)
4. Start iteration to compute damage parameters
   a. Calculate thermodynamic forces

(Eq. 6 & 7)
   b. Calculate damage parameters (Eq. 8)
   c. Update current stress (Eq. 1)
   d. Stop iteration when damage parameters have converged
5. Compute C and update stress (Eq. 1)
6. Use inverse of C as Jacobian

Next follows the corresponding treatment of the resin area. For the pure resin areas within the RVE a Ladevèze damage model [4] also has been used.
As mentioned above, the damage model for the pure resin material is very similar to the model used for UD composites. A basic difference is the fact that the resin material model is based on an isotropic material. Again it is assumed that the Poisson's ratio does not depend on the damage parameter. Hence, the strain-stress relation is given in equation (9). The thermodynamic force is defined in equation (10). Notice that the thermodynamic force is written in terms of strains instead of stress. Damage evolution is again based on active damage forces and can be computed according to the fibre bundles and Eq. 7 and 8.

$$
\begin{bmatrix} \varepsilon_{11} \\ \varepsilon_{22} \\ \varepsilon_{33} \\ \varepsilon_{12} \\ \varepsilon_{13} \\ \varepsilon_{23} \end{bmatrix} = \begin{bmatrix} \frac{1}{E_0(1-d)} & \frac{-\nu_0}{E_0(1-d)} & \frac{-\nu_0}{E_0(1-d)} & 0 & 0 & 0 \\ \frac{-\nu_0}{E_0(1-d)} & \frac{1}{E_0(1-d)} & \frac{-\nu_0}{E_0(1-d)} & 0 & 0 & 0 \\ \frac{-\nu_0}{E_0(1-d)} & \frac{-\nu_0}{E_0(1-d)} & \frac{1}{E_0(1-d)} & 0 & 0 & 0 \\ 0 & 0 & 0 & \frac{1}{G_0(1-d)} & 0 & 0 \\ 0 & 0 & 0 & 0 & \frac{1}{G_0(1-d)} & 0 \\ 0 & 0 & 0 & 0 & 0 & \frac{1}{G_0(1-d)} \end{bmatrix} \begin{bmatrix} \sigma_{11} \\ \sigma_{22} \\ \sigma_{33} \\ \sigma_{12} \\ \sigma_{13} \\ \sigma_{23} \end{bmatrix} \tag{9}
$$

$$
Z = \frac{E_0}{2}\left[\frac{(1-\nu_0)(\varepsilon_{11}^2 + \varepsilon_{22}^2 + \varepsilon_{33}^2) + 2\nu_0(\varepsilon_{11}\varepsilon_{22} + \varepsilon_{22}\varepsilon_{33} + \varepsilon_{11}\varepsilon_{33})}{(1+\nu_0)(1-2\nu_0)} + \frac{\varepsilon_{44}^2 + \varepsilon_{55}^2 + \varepsilon_{66}^2}{2(1+\nu_0)} \right] \tag{10}
$$

In order to arrive a procedure corresponding to the fibre bundles, we rewrite equation (9) as follows:

$$\varepsilon = C\sigma = \frac{1}{(1-d)}C_0\sigma \qquad (11)$$

and the strain energy density is again given by

$$W = \frac{1}{2}\sigma^T\varepsilon = \frac{1}{2}\sigma^T C\sigma \qquad (12)$$

The thermodynamic force is now formulated in term of strains instead of stress as follows:

$$Z = \frac{1}{2}\sigma^T \frac{\partial C}{\partial d}\sigma = -\frac{1}{2}\varepsilon^T \frac{\partial\left(C^{-1}\right)}{\partial d}\varepsilon \qquad (13)$$

Eq. 13 may be verified by using the fact that $C^{-1}C = I$. Since C^{-1} can be written as $(1-d)C_0^{-1}$ it is found that $\dfrac{\partial\left(C^{-1}\right)}{\partial d} = -C_0^{-1}$, which implies that the thermodynamic force depends only on the strains and not on the damage parameter. Using this result, the thermodynamic force is given by:

$$Z = \frac{1}{2}\varepsilon^T C_0^{-1}\varepsilon \qquad (14)$$

which is actually equal to the linear elastic strain energy and also equal to Eq. 10.

As mentioned before, the assumption that the Poisson's ratio is not affected by the damage parameter is questionable. However, in this specific case this assumption results in a very simple and numerically efficient formulation (see Eq. 14 and 17). When the Poisson's ratio also depends on the damage parameter, Eq. 17 becomes rather complicated and is no longer independent from the damage parameter. Since for the present formulation the thermodynamic force does not depend on the damage parameter, the computational procedure simplifies to:

1. Get current strain (input value)
2. Calculate thermodynamic forces (Eq. 13 or 17)
3. Calculate damage parameters (Eq. 8)
4. Compute C and update stress (Eq. 12)
5. Use inverse of C as Jacobian

The iterative loop to calculate the damage parameter can be omitted.

It is mentioned that the present model does not distinguish between tension and compression. However, in practice most resins show significant differences in failure behaviour between tension and compression.

2.4 Periodic boundary conditions

The RVE will be simulated as if it would be located in an infinitely large block of repeating RVE's. Six different boundary value problems will be solved for the RVE in order to predict the full anisotropic stiffness matrix.
For each boundary value problem Periodic Boundary Conditions (PBC's) are required to represent the fact that the RVE is located in an infinitely large block of repeating RVE's. In the existing implementation these boundary conditions are generated by means of a Python script and are defined as tying constraints. The definition of the PBC's will be discussed for two specific opposite faces. For other opposite faces similar PBC's are applied. Consider the face xz⁻, as shown in Fig. 2.5, and the opposite face xz⁺. Between all nodes on these faces, except the nodes on the red edges and all corner nodes, the following equations are defined:

$$u^{xz+} - u^{xz-} = u_C - u_A$$

where u denote the nodal displacement in x-direction. Similar equations are defined for displacements in y- and z-direction.
For nodes on the edges, except the corner nodes, the following constraints are defined:

$$u^{AB} - u^{FE} = u_C + u_D - 2u_A$$

Again, similar equations hold true for displacements in y- and z-direction.
Finally, the corner nodes are constrained by:

$$u_F - u_C = u_D - u_A$$

$$u_G - u_B = u_C - u_A$$

$$u_E - u_C = u_D + u_B - 2u_A$$

and equivalent equations for the remaining directions.

The reason that edges and corner nodes are excluded for the opposite faces is that otherwise some nodes will be overconstrained. If the constraints that hold true for the faces are written for all nodes without exceptions, the constraints for edges and corner nodes follow straightforwardly from these equations.

The RVE is loaded by prescribed displacements on the corner nodes A, B, C and D.

The present implementation of PBC's, see Fig. 2.5, requires matching meshes for all opposite faces.
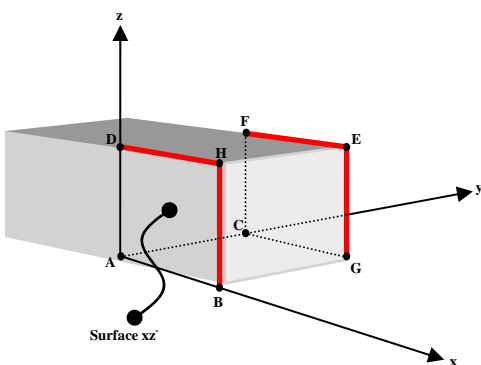
Fig. 2.5 Periodic boundary conditions

2.5 RVE example

In Fig. 2.6 an RVE for a braided composite is seen, with the meshed yarns visible, is seen ready for one of the above mentioned boundary value problems, with tension in the 1-1 direction. Fig. 2.7 shows a contour plot of the stress in the yarns in fibre direction. It can be seen the yarns carrying in the load direction display the higher stress. Fig. 2.8 shows a contour plot of the strain in the resin.
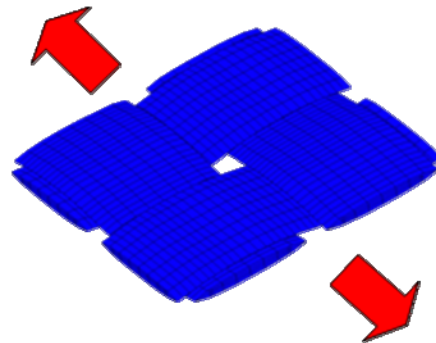
Fig. 2.6 RVE for braided composite, here with meshed yearns visible, ready for tensile load
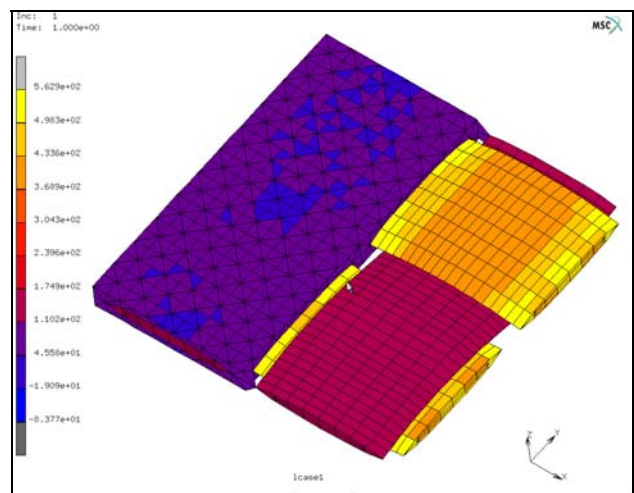
Fig. 2.7 RVE; stress in fibre direction in yearns; under tensile load
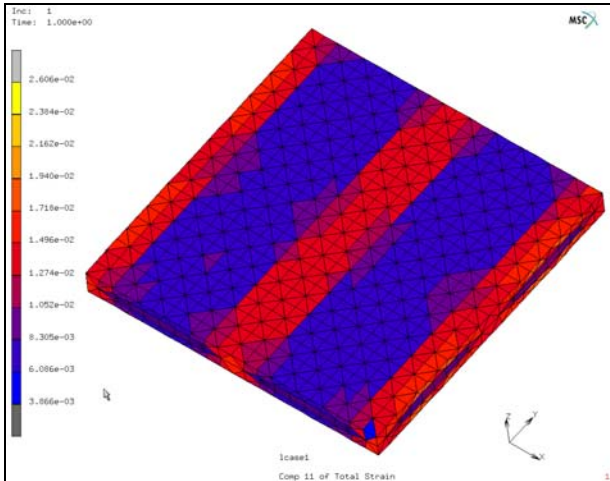
Fig. 2.8 Strain in resin in load direction

3 Next steps and applications

Currently the application is prepared for implementation into the macro level and in the first place solid elements and continuum shells are foreseen for engineering use.

Different fibre architectures are processed. Composite stiffening elements are currently targeted for validation on the macro level.

On the numerical side improvements are under way of the damage model, mainly pertaining to the treatment of the yarns. In addition to this, the implementation of completely new damage models are possible and considered, since the architecture of the numerical developments are totally modular.

4. Summary and Conclusions.

The paper describes the numerical treatment of various textile fibre reinforced composites, focusing on a nonlinear model for the simulation under mechanical loading up to damage of these materials.

The paper discussed the capturing of the fibre geometry by micro computer tomography. Subsequently the representative volume element, RVE, is treated, for the establishment of the geometry by Hypermesh, to the element meshing in ABAQUS.

In the RVE damage models on constituent level are discussed for the yarns and the resin.

The periodic boundary conditions, needed for the proper description of the RVE are subsequently described. Finally an example of en RVE, under uniaxial tensile loading is given.

Improvements in the numerical procedure are under way in terms of details, discussed in connection with the damage models used here. Implementation of different damage models are as well possible.

The practical use is foreseen in connection with development of various textile fibre reinforced composites, braided materials thereby planned to have certain priority in the nearest future. Further fibre architectures are planned to be added subsequently.

References

[1] Verpoest, I. & Lomov, S. V., Virtual textile composites software WiseTex: Integration with micro-mechanical, permeability and structural analysis Composites Science and Technology, pp 2563-2574, 2005.

[2] Middendorf, P. van den Broucke, B, Linde, P., texComp, modelling and Simulation of textile reinforced composites, Internal technical report, Airbus, 2009.

[3] Stössel, R., Günther, T., Dierig, T., Schladitz, K., Godehardt, M., Kessling, P.-M., µ-Computed Tomography for micro-structure characterization of CFRP, QNDE Conference, San Diego, 2010.

[4] Ladevèze, P. Lemaitre, J. (Ed.) Chapter 10.6: A Damage Mesomodel of Laminate Composites, San Diego (Calif.): pp. 1004-1014, Academic press, 2001.

Copyright Statement